Electrochemical Reduction of Quinones: Interfacing Experiment and Theory for Defining Effective Radii of Redox Moieties†

Duoduo Bao,[‡,§] Sangeetha Ramu,[‡] Antonio Contreras,[‡] Srigokul Upadhyayula,[‡,§] Jacob M. Vasquez,[‡,§] Gregory Beran,*[,⊥] and Valentine I. Vullev*[,‡,§,⊥]

Department of Bioengineering, University of California, Riverside, California 92521, Center for Bioengineering Research, University of California, Riverside, California 92521, and Department of Chemistry, University of California, Riverside, California 92521

Received: February 26, 2010; Revised Manuscript Received: May 16, 2010

Using cyclic voltammetry, we examined the dependence of the reduction potentials of six quinones on the concentration of the supporting electrolyte. An increase in the electrolyte concentration, resulting in an increase in the solution polarity, caused positive shifts of the reduction potentials. We ascribed the observed changes in the potentials to the dependence of the solvation energy of the quinones and their anions on the media polarity. Analysis of the reduction potentials, using the Born solvation energy equation, yielded unfeasibly small values for the effective radii of the quinone species, that is, the experimentally obtained effective radii were up to 4-fold smaller than the radii of the solvation cavities that we calculated for the quinones. The nonspherical shapes of the quinones, along with the uneven charge density distribution in their anions, encompassed the underlying reasons for the discrepancies between the obtained experimental and theoretical values for the radii of these redox species. The generalized Born approach, which does not treat the solvated species as single spheres, provided means for addressing this discrepancy and yielded effective radii that were relatively close to the measured values.

Introduction

This article describes an electrochemistry study of benzo- and naphthaquinones. Our findings reveal a pronounced dependence of the quinone reduction potentials on the concentration of the supporting electrolyte. An increase in the electrolyte concentration causes a positive shift in the values of the measured reduction potentials of the quinones. We ascribe the observed positive shifts to the electrolyte-induced increase in the media polarity. The Born solvation energy, estimated via the widely used spherical approximation for molecular ions, fails to quantify the observed trends. As an alternative, a generalized Born approach,[1,2] which represents molecular species as collections of spheres, yields results that agree with the experimental findings and demonstrates plausible means for addressing the potential deficiencies with the single-sphere approximation of organic ions.

Electron-transfer processes play a key role in chemical and biological systems.[3−23] Photoinduced electron transfer represents the central paradigm of light−energy conversion, for example, of photosynthesis[24−31] and of photovoltaics.[32−39] The Rehm−Weller equation allows for estimation of the thermodynamic driving force, that is, the change in the Gibbs energy, $\Delta G_{et}^{(0)}$, of photoinduced charge-transfer processes, by employing readily measurable quantities such as the redox potentials of electron donors and acceptors.[40−42]

A significant portion of the values of measured standard redox potentials (essential for estimation of $\Delta G_{et}^{(0)}$) encompasses a contribution of the solvation of the charged species involved in the electron-transfer processes. The Born equation for the electrostatic component of the solvation energy, ΔG_S, of spherical ions with radius R and charge Z, in a medium with dielectric constant ε, is $\Delta G_S = -Z^2e^2(8\pi\varepsilon_0 R)^{-1}(1 - \varepsilon^{-1})$.[43,44] The Born expression allows for quantification of the solvation contribution to the redox potentials, and it is introduced as a correction term in the Rhem−Weller equation in order to relate thermodynamic data acquired for media with different polarities.[42]

Assuming a spherical shape for the ionic species, however, presents an important approximation in the Born solvation energy expression. For metal ions and for a range of chelates, such a single-sphere approximation is acceptable. Very few organic molecules and protein cofactors, however, have shapes that resemble spheres. Therefore, for estimation of the energetics of electron-transfer systems comprising nonspherical redox species, the assignment of the values of effective radii involves nontrivial assumptions.

Experimentally obtained molecular volumes provide means for estimation of effective radii, assuming spherical shape of the solute species. For example, molecular volumes, obtained from mass density, sound velocity, or refractivity measurements, allow for estimation of "average" effective radii.[45−57] Diffusivity characteristics of molecules and their ions yield values for their effective Stokes radii,[58−74] which represent their mass-transport properties.[75] Alternatively, from X-ray or NMR structural data, the radius of a spherical solvation cavity can be ascribed to the distance from the center of mass of the solvated molecule to its most distal van der Waals boundary.[76−78] For moieties with highly irregular shapes, however, this approach provides dimensions that are an overestimation of the effective radii, reflecting their redox and charge-transfer behavior observed experimentally. Fitting such molecular species into ellipsoid cavities allows for representing the effective radii as averages of the three

† Part of the "Michael R. Wasielewski Festschrift".

* To whom correspondence should be addressed. vullev@ucr.edu (V.I.V.); gregory.beran@ucr.edu (G.B.).

‡ Department of Bioengineering.

§ Center for Bioengineering Research.

⊥ Department of Chemistry.

10.1021/jp101730e
Published on Web 06/09/2010

SCHEME 1: Quinones Used for This Study

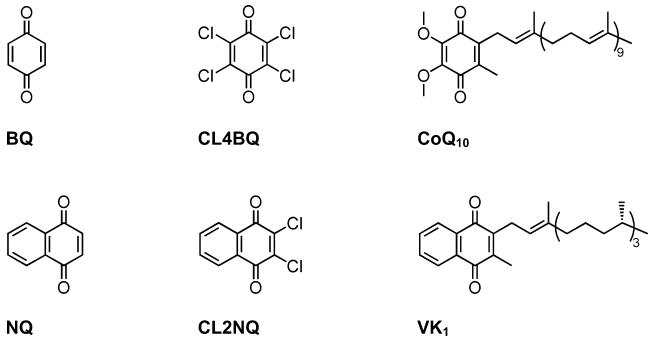

ellipsoid axes.[79] Even this approach of averaging the length, width, and height of such molecular moieties can overestimate the effective radii for molecular ions with localized charges.[80−83]

Although reaction field theory allows for analytical and numerical solutions for the solvation energies of species with, respectively, ellipsoid and arbitrary shapes,[84−89] the significant increase in the number of parameters appears to prevent their use for analysis of charge-transfer systems. The commodity of representing the molecular dimensions with a single parameter — an effective radius — underlines the need for relating this parameter with the structural features of the molecular ions.

Herein, we examine the relation between the effective radii of quinone derivatives (obtained electrochemically) and their molecular dimensions. Using cyclic voltammetry, we examined the solvation-induced trends in the redox properties of six quinones (Scheme 1). Varying the concentration of the supporting electrolyte allowed for inducing changes in the medium polarity.[42] An increase in the solution polarity indeed caused positive shifts in the reduction potentials of the quinones. We ascribed the observed effects to the dependence of the quinone solvation energy on the media polarity. The long aliphatic chains attached to the quinone rings did not provide notable contribution to the solvation stabilization of the quinones, that is, the dependence of the reduction potentials of coenzyme Q_{10} and vitamin K_1 on the media polarity was similar to the media polarity dependence for 1,4-benzoquinone and 1,4-naphthaquinone, respectively (Scheme 1).

Adopting the single-sphere approximation for the Born solvation energy (eq 2) failed to feasibly quantify the trends in the reduction properties of the quinones induced by the variations in the media polarity. Via applying the Born relation to the redox data (eqs 1b and 2b), we obtained effective radii for all six quinones that were unfeasibly small. The thus experimentally obtained effective radii were up to 4-fold smaller than the theoretical values for the radii that we obtained from ab initio calculations of the corresponding molecular volumes. Alternatively, a generalized Born approach, which does not treat the charged molecular species as spherical entities,[1,2,90−95] manifested a good agreement with the experimental findings. Further examination revealed that the charge localization was the principle underlying reason for the observed discrepancy between theory and experiment.

Results and Discussion

Accounting for Solvation in Redox Processes. The solvation energy dependence of the redox potential, $E^{(0)}$, of an n-electron reduction of species, A, with a charge Z, is

$$A^Z + ne^{-1} \rightarrow A^{Z-n} \tag{1a}$$

$$E^{(0)} = E^{(0,ns)} + \frac{\Delta G_S^{(0)}}{nF} \tag{1b}$$

where $E^{(0,ns)}$ is the standard redox potential in the absence of solvation, F is the Faraday constant, and $\Delta G_S^{(0)}$ represents the change in the solvation of species A upon the alteration of their charge

$$\Delta G_S^{(0)} = \frac{e^2}{8\pi\varepsilon_0}\left(\frac{(Z-n)^2}{R_{Red}} - \frac{Z^2}{R_{Ox}}\right)\left(1 - \frac{1}{\varepsilon}\right) = \frac{\Xi_{Red} - \Xi_{Ox}}{8\pi\varepsilon_0} \times \left(1 - \frac{1}{\varepsilon}\right) \tag{2a}$$

where e is an elementary charge, ε_0 is the dielectric permittivity of vacuum, and R_{Red} and R_{Ox} are defined as the radii of the cavities that accommodate, respectively, the reduced, A^{Z-n}, and the oxidized, A^Z, species. The charge-to-size ratios, Ξ_{Red} and Ξ_{Ox}, for the reduced and oxidized species, respectively, have units of charge squared over distance. Assuming negligible change in the size of A^Z upon reduction, that is, $R = R_{Red} \approx R_{Ox}$, allows for simplifying of the solvation energy correction term for the redox potential, $E^{(0)}$

$$\Delta G_S^{(0)} \approx \frac{(n - 2Z)ne^2}{8\pi\varepsilon_0 R}\left(1 - \frac{1}{\varepsilon}\right) \tag{2b}$$

These expressions (eqs 1b and 2b) depict two important trends for the redox properties of noncharged species (eq 1a); (1) an increase in the media polarity results in negative shifts in the oxidation potentials and positive shifts in the reduction potentials, and (2) the redox potentials of smaller species are more susceptible to changes in the media polarity. The former trend is readily explained by the fact that polar media stabilize charged species. For reduction of electroneutral species, the oxidized form is charged. An increase in the media polarity, therefore, drives the redox equilibrium toward the oxidized form and increases the reducing potency of the species, and hence, it results in negative shifts in the standard redox potential. A similar argument stands for the reduction potentials of electroneutral species, for which the reduced form is negatively charged (eq 1a). The latter trend reflects the electrostatic requirement for increased electric field density, generated by fewer media dipoles, to stabilize a charge confined in a smaller solvation cavity, that is, a decrease in R requires an increase in ε to achieve the same electrostatic "screening" of the confined charge.

We have previously demonstrated the dependence of the redox potentials of ferrocene and of an aminonaphthalimide derivative on the media polarity.[42] The oxidation potential of ferrocene shifted toward more negative values upon an increase in the electrolyte concentration and in the polarity of the organic solvents used.[42] Concurrently, the reduction potential of the aminonaphthalimide shifted toward more positive values as the media polarity increased.[42]

Quinone Reduction. Due to their large electron affinities,[96−99] quinones represent a widely preferred choice for electron acceptors in synthetic charge-transfer systems.[100−109] Furthermore, derivatives of quinones have key importance for biological redox processes, such as photosynthesis and cellular respiration.[110−115] For example, two plastoquinones, derivatives of 2,3-dimethyl-1,4-benzoquinone with long aliphatic chains, are a part of the electron-transfer chain of Photosystem II, and one of them, Q_B, provides means for

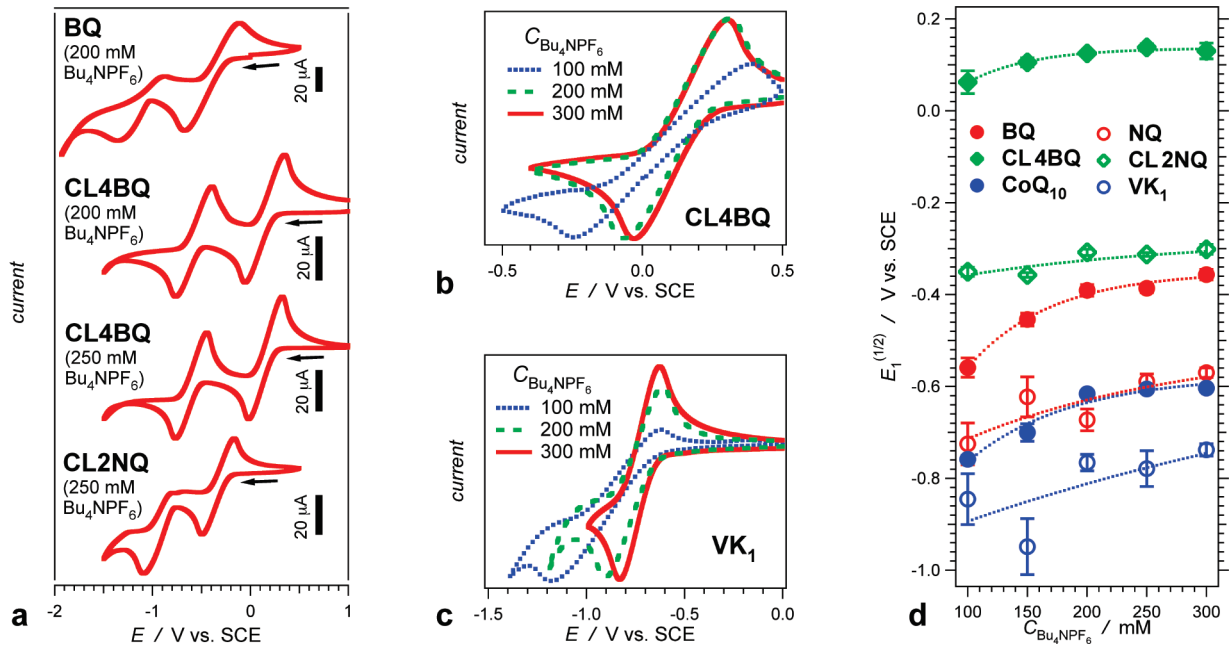

Figure 1. Dependence of the electrochemical reduction of quinones on the electrolyte concentration for chloroform media (quinone concentration = 2 mM; scan rate = 50 mV/s). (a) Cyclic voltammograms of three quinones for two different electrolyte concentrations. (b, c) Cyclic voltammograms displaying the first reduction waves of two quinones for three different electrolyte concentrations. The cathodic peaks are normalized for visualizing the trends. (d) Dependence of the quinone first-wave reduction potentials on the electrolyte concentration.

transmembrane proton transport via double reduction/oxidation.[116−121] Similar quinones mediate the same functions in the bacterial photosynthetic reaction center.[122−126] Ubiquinones, also known as coenzyme Q, derivatives 2,3-dimethoxy-5-methyl-1,4-benzoquinone, also with long aliphatic chains, are a key component of the respiratory electron-transport chain.[127−132] Among them, coenzyme Q_{10} is the most abundant quinone in the human mitochondria, and it has significant health implications.[133−141] (The subscript 10 refers to the number of isoprenylene units in the aliphatic chain (Scheme 1).)

Photosynthesis and respiration are not the only biological processes that take advantage of the redox properties of quinones. For example, a group of lipophilic vitamins, denoted as vitamin K, derivatives of 2-methyl-1,4-naphthaquinone with long aliphatic chains (Scheme 1), are essential for post-translational carboxylation of glutamates in certain proteins involved in the blood coagulation cascade[142−145] and in mineralization of tissues such as bone and dentin.[146−150]

The two one-electron reduction steps of quinones are characterized with standard redox potentials $E_1^{(0)}$ and $E_2^{(0)}$

$$Q + e^- \rightarrow Q^- \qquad E_1^{(0)} \tag{3a}$$

$$Q^- + e^- \rightarrow Q^{2-} \qquad E_2^{(0)} \tag{3b}$$

Accordingly, the cyclic voltammograms revealed two distinct reduction steps for the investigated quinones (Figure 1a).[79,151−153] Because of the reversibility of the investigated electrochemical reduction steps, we used the half-wave potentials instead of the corresponding standard reduction potentials for our analysis, that is, $E_t^{(1/2)} \approx E_t^{(0)}$.

The choice of solvent and electrolyte for the electrochemical measurements was driven by two factors essential for this study, (1) no hydrogen-bonding capabilities and (2) low media dielectric constants. The redox properties of quinones are sensitive to protonation of the phenolate oxygens of Q^- and Q^{2-} (eq 3).[151,152] Therefore, using a solvent and an electrolyte that cannot form hydrogen bonds or chelate oxygens ensured that the observed changes in the redox properties did not result in specific interactions involving the quinone oxygens.

The media polarity, γ, is inversely proportional to the negative value of its dielectric constant, ε, that is, $\gamma = (n^{-2} - \varepsilon^{-1})$, where n is the index of refraction and n^2, hence, is viewed as the dynamic dielectric constant of nonmagnetic media. The differences between the refractive indexes of the used electrolyte solutions, however, are negligible (Table 1). For this study, therefore, the dielectric properties of the solutions account for their polarities.

The Born solvation energy has a similar dependence as γ on the dielectric properties of the media, that is, $\Delta G_S \propto 1 - \varepsilon^{-1}$ (eq 2).[43,44] A solvent with a relatively small dielectric constant ought to exhibit relatively large changes not only in ε but also in ε^{-1} upon addition of electrolyte. Therefore, the use of electrolyte solutions in nonpolar solvent allows for exploration of a relatively broad range of ε^{-1} and ΔG_S.

On the basis of the above two considerations, that is, no hydrogen bonding and low polarity, we chose chloroform solutions of tetrabutylammonium hexafluorophosphate (Bu_4NPF_6) with different concentrations. Use of chloroform, however, posed a limitation due to its relatively narrow redox window. The Faradaic currents, resultant from the reduction of chloroform, became apparent at potentials more negative than about −1.5 V versus SCE (Figure 1a). Therefore, in this study, we focused predominantly on the first one-electron reduction of the quinone species, that is, on $E_1^{(1/2)}$ (eq 3a).

The reduction potentials of all six quinones manifested dependence on the electrolyte concentration, $C_{Bu_4NPF_6}$ (Figure 1b, c, d). Exponential fits allowed us to extrapolate the reduction potentials for the neat solvent, that is, for $C_{Bu_4NPF_6} = 0$ (Table 1).[42] As we have demonstrated, the use of such extrapolated values for the redox potentials in the Rehm−Weller equation proves immensely convenient for estimation of the charge-transfer driving forces by considering solely the dielectric

TABLE 1: First Half-Wave Reduction Potentials of Quinones, $E_1^{(1/2)}$, for Chloroform Electrolyte Solutions with Different Concentrations[a]

	concentration of Bu_4NPF_6					
quinone	0 mM[b], ($\varepsilon = 4.77$), ($n = 1.447$), ($\gamma = 0.268$)[d]	100 mM, ($\varepsilon = 11.8$)[c], ($n = 1.448$), ($\gamma = 0.392$)[d]	150 mM, ($\varepsilon = 13.6$)[c], ($n = 1.448$), ($\gamma = 0.404$)[d]	200 mM, ($\varepsilon = 15.9$)[c], ($n = 1.447$), ($\gamma = 0.415$)[d]	250 mM, ($\varepsilon = 16.5$)[c], ($n = 1.446$), ($\gamma = 0.417$)[d]	300 mM, ($\varepsilon = 17.1$)[c], ($n = 1.446$), ($\gamma = 0.420$)[d]
BQ	-1.24 ± 0.26	-0.559 ± 0.021	-0.454 ± 0.014	-0.391 ± 0.012	-0.387 ± 0.009	-0.357 ± 0.011
CL4BQ	-0.341 ± 0.226	0.062 ± 0.025	0.105 ± 0.009	0.125 ± 0.006	0.138 ± 0.008	0.130 ± 0.017
CoQ_{10}	-1.17 ± 0.30	-0.749 ± 0.009	-0.700 ± 0.019	-0.616 ± 0.008	-0.605 ± 0.004	-0.604 ± 0.005
NQ	-0.857 ± 0.397	-0.725 ± 0.045	-0.622 ± 0.043	-0.673 ± 0.024	-0.590 ± 0.017	-0.570 ± 0.010
CL2NQ	-0.413 ± 0.160	-0.350 ± 0.010	-0.358 ± 0.005	-0.308 ± 0.007	-0.313 ± 0.004	-0.302 ± 0.010
VK_1	-0.995 ± 0.258	-0.846 ± 0.055	-0.949 ± 0.061	-0.766 ± 0.018	-0.779 ± 0.039	-0.738 ± 0.013

[a] The values of $E_1^{(1/2)}$, in V versus SCE, for 100−300 mM Bu_4NPF_6 were obtained from cyclic voltammetry data (Figure 1). The error bars represent a 90% confidence level from two-sided Student *t*-analysis. [b] The values of $E_1^{(1/2)}$ for neat chloroform, that is, 0 mM Bu_4NPF_6, were obtained from monoexponential extrapolation to 0 (Figure 1d). The error bars represent a single standard deviation as yielded from the least-squares fits. [c] The dielectric constants for the electrolyte solutions were extracted from fluorescence solvatochromism data (Figure 2). [d] $\gamma = n^{-2} - \varepsilon^{-1}$.

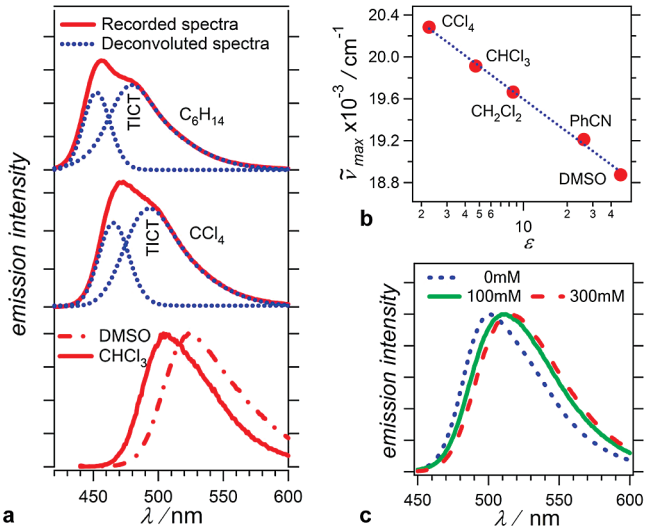

Figure 2. (a) Solvatochromism of the fluorescence of Ph-ANI observed for solvent media with different polarity, dimethylsulfoxide (DMSO), benzonitrile (PhCN), dichloromethane (CH_2Cl_2), chloroform ($CHCl_3$), tetrachloromethane (CCl_4), and hexane (C_6H_{14}). (a) Fluorescence spectra of Ph-ANI (10 μM) for solvents with different polarity ($\lambda_{ex} = 410$ nm; intensities normalized at $\lambda_{em}^{(max)}$). The shoulders of the spectral bands, collected for the nonpolar solvents (CCl_4 and C_6H_{14}), suggested multiple components and hence were deconvoluted. The broad red-shifted components, obtained from the deconvolution, were ascribed to the radiative deactivation of the TICT state.[157−160] Similar deconvolution algorithms did not yield multiple components for the Ph-ANI spectra recorded for the rest of the solvents. (b) Dependence of the spectral maxima on the dialectic constant of the solvents for solvents with similar indexes of refraction, that is, $n_{CCl_4} = 1.46$; $n_{CHCl_3} = 1.45$; $n_{CH_2Cl_2} = 1.42$; $n_{PhCN} = 1.53$; and $n_{DMSO} = 1.48$. For CCl_4, the maximum of the red-shifted TICT band was used. (c) Fluorescence spectra of Ph-ANI recorded for chloroform solutions with different concentrations of Bu_4NPF_6. From the concentration dependence of the fluorescence maxima and the calibration curve, shown in (b), the dielectric constants of the electrolyte solutions were extracted.[42]

properties of the neat solvents (rather than of the electrolyte solution) for the Born correction term.[42]

Polarity of the Electrolyte Solutions. We ascribed the observed electrolyte concentration dependence of the reduction potentials to the variations of the dielectric properties of the chloroform solutions. An increase in the concentration of the supporting electrolyte increases the dielectric constant of the chloroform solutions[154] and hence of $\Delta G_S^{(0)}$, causing positive shifts in the values of $E^{(0)}$ (eqs 1b and 2).

The fluorescence solvatochromism of *N*-phenyl-4-dimethylamino-1,8-naphthalimide (Ph-ANI), which can be readily prepared in two synthetic steps,[42,155,156] allowed us to determine the dielectric constants of the electrolyte solutions.[42] For nonpolar solvents (such as tetrachloromethane and hexane, which do not have a permanent molecular dipole moment), the fluorescence spectra of Ph-ANI revealed two overlapping bands (Figure 2a). For relatively polar solvents, however, the Ph-ANI fluorescence spectra exhibited a single band, which shifted to the red with an increase in the media polarity (Figure 2a).

The observed spectral behavior of Ph-ANI was consistent with the formation of a twisted intramolecular charge-transfer (TICT) excited state[157−160] involving the electron-donating dimethylamine group attached to the electron-withdrawing naphthalimide.[161,162] For dialkylamine aromatic chromophores, two opposing effects determine the dihedral angle of the arylamine C−N bond. While the conjugation of the amine free electron pair with the aromatic π-system stabilizes the planar conformation, the steric hindrance between the alkyls and the aromatic ring drives toward a twisted conformation. Upon excitation, the move of an electron to an orbital with antibonding character decreases the strength of the amine−aryl π-conjugation, increasing the preference for the twisted conformation. Although the π-conjugation polarizes the dialkylamine aromatic moieties, the charge-transfer character of the twisted states results in increased polarization and pronounced solvatochromism.

For nonpolar media, while the blue-shifted fluorescence of Ph-ANI was ascribed to the decay from an excited state with a conformation close to the conformation of the ground state, the red-shifted fluorescence was ascribed to a radiative transition from a TICT state (Figure 2a). An increase in the media polarity stabilized the polar TICT state, causing the observed red shift of the fluorescence. Furthermore, such polarity-induced lowering of the energy of the charge-transfer state made the TICT conformer the predominant source for the radiative decay, resulting in the single-band fluorescence spectra observed for relatively polar solvents (Figure 2a).

The TICT fluorescence of Ph-ANI manifested a strong dependence on the dielectric properties of the media (Figure 2b).[42,161] This dependence allowed us to estimate the dielectric constants of the chloroform Bu_4NPF_6 solutions (Figure 2b, c). Our findings revealed about a 4-fold increase in the dielectric constant with an increase in the electrolyte concentration, $C_{Bu_4NPF_6}$, from 0 to 300 mM (Figure 2c, Table 1). The measured refractive index, however, showed only a 0.05−0.1% decrease with the addition of the electrolyte.

Correlation between Reduction Potentials and Solvent Dielectric Properties. The difference between the reduction potentials, measured for $C_{Bu_4NPF_6} = 100$ and 300 mM demon-

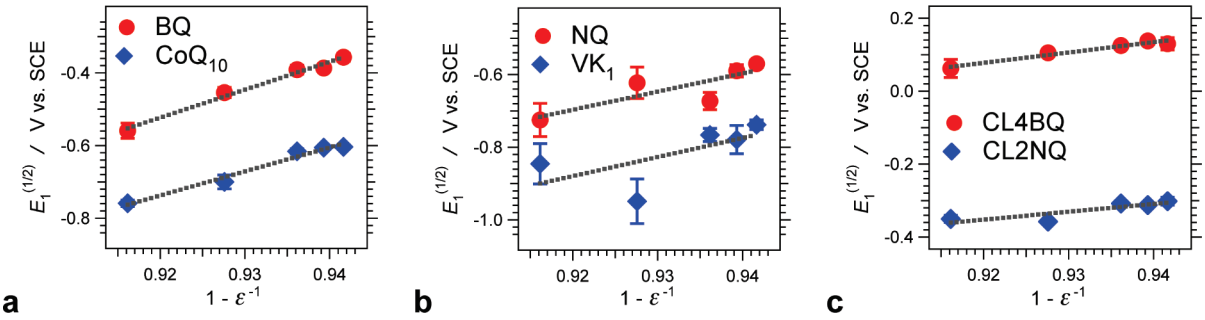

Figure 3. Dependence of the quinone first-wave reduction potentials on the inverted dielectric constant of the electrolyte media. The dotted lines represent least-squares linear fits with the following correlation coefficients, R: (a) for BQ, $R = 0.993$, and for CoQ_{10}, $R = 0.987$; (b) for NQ, $R = 0.825$, and for VK_1, $R = 0.650$; and (c) for CL4BQ, $R = 0.976$, and for CL2NQ, $R = 0.875$.

TABLE 2: Effective Radii of Quinones Obtained from Electrochemical Data and from Ab Initio Calculations

quinone	R_{eff} / Å[a]	$R_{eff}^{(GB)}$ / Å[b]	$R_{sph}^{(Q)}$ / Å[c]	$R_{sph}^{(Q^{\bullet-})}$ / Å[d]	Δgb[e]	Δsph[f]	Δsph / Δgb
BQ	0.935	1.67	3.99	4.06	0.786	3.34	4.25
CL4BQ	2.53	2.47	4.58	4.63	0.0237	0.830	35.0
CoQ_{10}	1.09	2.59[g]	5.31[g]	5.35[g]	1.38	3.91	2.84
NQ	1.44	2.00	4.43	4.50	0.389	2.13	5.46
CL2NQ	3.35	2.44	4.68	4.73	0.272	0.412	1.52
VK_1	1.38	2.44[g]	5.26[g]	5.32[g]	0.768	2.86	3.72

[a] Effective radii, R_{eff}, of the singly reduced quinone ions from electrochemical data, assuming spherical approximation (eq 4, Figure 3). [b] Effective sizes for one-electron reduction, $R_{eff}^{(GB)}$, calculated using the generalized Born approach (eq 6). Atoms were approximated to spheres with homogeneously distributed partial charges. The atomic radii and atomic charges were obtained from ab initio calculated structures (Figure 4). [c] Effective radii, $R_{sph}^{(Q)}$, of the noncharged quinone molecules from ab initio calculations, assuming spherical approximation. The standard deviations did not exceed 0.7 pm. [d] Effective radii, $R_{sph}^{(Q^{\bullet-})}$, of the singly reduced quinone ions from ab initio calculations, assuming spherical approximation. The standard deviations did not exceed 0.7 pm. [e] Δgb represents the relative difference between the experimentally measured effective radii and the calculated GB effective radii, $\Delta gb = (|R_{eff} - R_{eff}^{(GB)}|)/R_{eff}$. [f] Δsph represents the relative difference between the experimentally measured effective radii and the calculated radii of the solute spherical cavities for the anions, $\Delta sph = (|R_{eff} - R_{sph}^{(Q^{\bullet-})}|)/R_{eff}$. [g] These values were obtained from ab initio calculations, employing a reduced basis set on structures with truncated aliphatic chains, that is, CoQ_{10} and VK_1 containing only one isoprenylene unit attached to their rings (Scheme 2, Figure 5).

strated the extent of dependence of the redox properties of the quinones on the electrolyte concentration (Table 1). The reduction of 1,4-benzoquinone (BQ) manifested the strongest dependence on the amount of electrolyte in the media (Table 1), which was consistent with its smallest molecular size in comparison with the other quinones (Scheme 1), that is, the smallest effective cavity radius, R (eq 2b).

The reduction potentials of the largest quinones, coenzyme Q_{10} (CoQ_{10}) and vitamin K_1 (VK_1) (Scheme 1), however, did not manifest the smallest dependence on the electrolyte concentration (Table 1). Hence, the aliphatic chains attached to the quinone rings did not contribute significantly to the effective radii, R_{Ox}, R_{Red}, or R, of the species (eq 2).

We observed the smallest dependence of $E_1^{(1/2)}$ on $C_{Bu_4NPF_6}$ for the two chlorinated quinones, 2,3-dichloro-1,4-naphthaquinone (CL2NQ) and 2,3,5,6-tetrachloro-1,4-benzoquinone (CL4BQ) (Table 1). The redox behavior of both chlorinated species manifested almost the same dependence on $C_{Bu_4NPF_6}$, implying that the addition of four chlorines to BQ (i.e., to yield CL4BQ) has a charge-stabilization effect similar to the addition of two chlorines and four carbons (i.e., to yield CL2NQ). The chlorine substituents, indeed, had a more dramatic effect than the alkyl and methoxy substituents of CoQ_{10} and VK_1 (Scheme 1). The larger size of the third-period chlorine, in comparison with the size of the second-period elements, carbon and oxygen, provides a plausible explanation for these trends. Furthermore, unlike the chlorine substituents, the alkyls do not contribute efficiently toward expanding the π-conjugation of the quinones and delocalizing the negative charges of their molecular ions.

The Born solvation-energy expression reveals the dependence of the redox potentials on the media dielectric constant (eqs 1b and 2a). For the first one-electron reduction step of the quinones (i.e., $Z = 0$ and $n = 1$), the dependence of the oxidation potential on the reciprocal dielectric constant is

$$E_1^{(1/2)} = E_1^{(1/2,ns)} + \frac{e^2}{8F\pi\varepsilon_0 R_{eff}}\left(1 - \frac{1}{\varepsilon}\right) \qquad (4)$$

Plots of half-wave reduction potentials versus $(1 - \varepsilon^{-1})$ indeed revealed linear correlations (Figure 3). The slopes of these linear fits yielded the effective radii, $R_{eff} = R_{Red}$ (eqs 2a and 4), of the quinone radical anions (eq 3a). The obtained values for R_{eff}, however, were unfeasibly small for spherical cavities that could accommodate the reduced quinones (Table 2). Nevertheless, it should be noted that the values of R_{eff} represented effective radii, which, although correlated to the size of the molecular ions, are not necessarily true radii.

Previous reports about the solvent dependence of the reduction of quinones failed to correlate the measured potentials, $E_1^{(0)}$, with the reciprocal values of the dielectric constant of the media, ε^{-1}, which is directly proportional to the Born solvation energy.[163] The reported quinone reduction potentials, however, manifested linear correlation with the electrophilicity of the used solvents, empirically expressed as a Gutmann acceptor number,[164−169] that is, an increase in the solvent electrophilicity stabilized the negatively charged semiquinones, causing the observed positive shifts of their reduction potentials.[163] We ascribe the reported failure to directly correlate the solvation energy with the shifts in the reduction potentials to (1) the use of ferrocene oxidation as an internal standard, while the redox properties of ferrocene strongly depend on the media polarity[42] and (2) the use of the dielectric values of the neat organic solvents for the electrolyte

SCHEME 2: Analogues of CoQ_{10} and VK_1 with Truncated Aliphatic Chains with the Corresponding CHELPG Charges of the Non-Hydrogen Atoms (in atomic units)

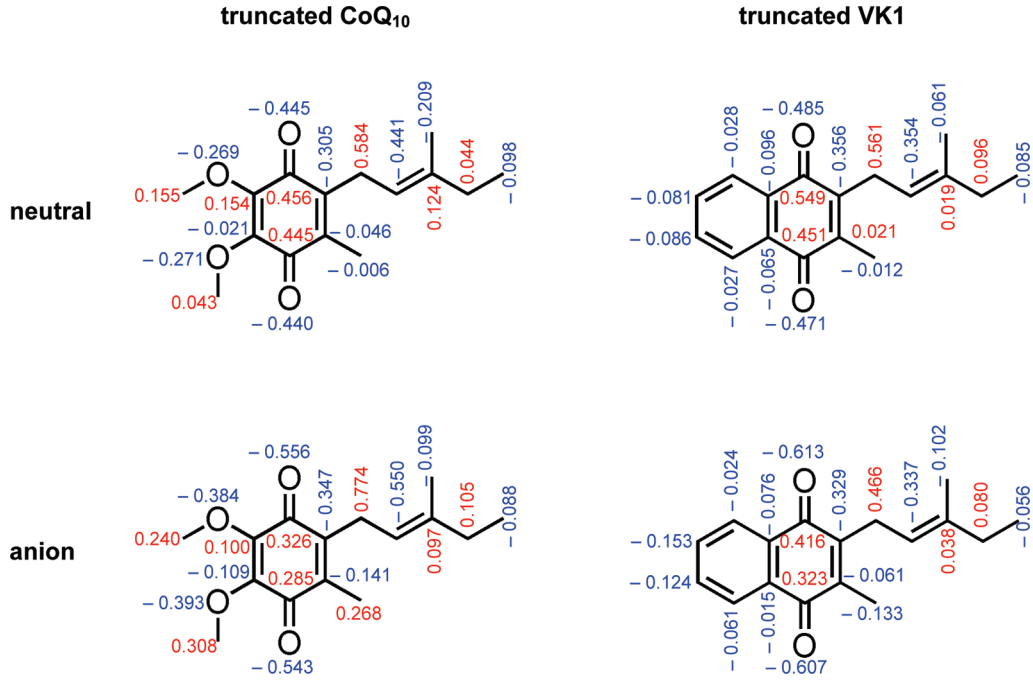

solutions employed for the electrochemical measurements, while, especially for nonpolar solvents, dissolved electrolytes increase the dielectric permittivity of the media.[42]

The values that we obtained for the effective radii, R_{eff}, of the reduced quinones exhibited several trends. The effective sizes of the reduced 1,4-naphthaquinone (NQ) and VK_1 were identical (Table 2), suggesting that the addition of the alkyl chains to the naphthaquinone ring system did not notably perturb the electrostatic interactions of the generated molecular ions with the dielectric media. The effective size of the $CoQ_{10}^{\bullet -}$ ion only slightly exceeds the size of $BQ^{\bullet -}$. This slight size increase could be ascribed to the two π-conjugating methoxy substituents in CoQ_{10}, rather than to the methyl and the long aliphatic chains (Scheme 1).

These findings have a key implication on the manner of defining the size parameter, R, in the Born solvation energy terms. According to the electrostatic model, the effective radius corresponds to the size of a spherical cavity around the charged species.[44] Functional groups, such as aliphatic chains, on which the charges do not reside, did not to contribute to the cavity size of the molecular ions. For the spherical approximation, therefore, such electronically nonconjugated substituents appear as a part of the solution media, rather than as a part of the molecular ion encapsulated in the solute cavity. Viewing molecular components as a part of the surrounding media, however, places challenges on the dielectric continuum approach for the Born solvation energy treatment, that is, it requires an introduction of either separate terms for the solution and for the molecular dielectric constants or a correction factor for the solution dielectric constant.

Theoretical Values of the Effective Radii. From ab initio calculations, we estimated the effective radii of the spherical cavities for BQ, CL4BQ, NQ, and CL2NQ. For CoQ_{10} and VK_1, we conducted the ab initio calculations on analogous structures with truncated aliphatic chains (Scheme 2). We used Monte Carlo integration of the density within a 0.001 electrons/bohr^3 cutoff for determining the molecular volumes of the quinones. From the volumes, the spherical radii were calculated. We applied an empirical correction to the calculated radii that predict reasonable solute cavity sizes for implicit solvent modeling.[170]

These calculated cavity radii, $R_{sph}^{(Q)}$ and $R_{sph}^{(Q^{\bullet -})}$, for the quinones and their anions, respectively, exceed the electrochemically measured effective radii by a factor of 1.5−4.9 (Table 2). This discrepancy was more pronounced for BQ and NQ than that for the chloroquinones, CL4BQ and CL2NQ, which agrees well with the notion for charge localization. While the negative charges of the radical anions were localized predominantly on the two oxygens of $BQ^{\bullet -}$ and $NQ^{\bullet -}$, in $CL4BQ^{\bullet -}$ and $CL2NQ^{\bullet -}$, the charges were also distributed over the peripheral chlorines (Figure 4).

For CoQ_{10} and VK_1, the sizes of the solute cavities strongly depend on the conformation of the flexible aliphatic and methoxy chains. Geometry optimization calculations produced conformations for CoQ_{10} and VK_1, in which the flexible chains folded over the aromatic rings (Figure 5). While intramolecular van der Waals interactions can explain the preference for such a folded conformation in vacuum, the abundance of the extended conformers for favorable solution media should not be overlooked. Therefore, the interpretation of solute−cavity radii for moieties with flexible side chains should be approached with caution.

Possible sources for the discrepancy between the experimentally obtained effective radii and the physically realistic molecular dimensions (confirmed with the radii of the solvation cavities of the quinones) include the assumptions for (1) the single-sphere approximation of the shape of the molecular anions, (2) homogeneous charge density distribution throughout the molecular volume, and (3) the correlation of the interfacial electrochemical thermodynamics with the bulk dielectric properties of the supporting electrolyte.

Interfacial Properties of the Working Electrode. To examine the environment of the interfacial redox processes, we employed impedance spectroscopy (IS). IS allowed us to characterize the capacitance of the double layer on the working electrode for different electrolyte concentrations and for different applied potentials. For the IS data analysis, we modeled the

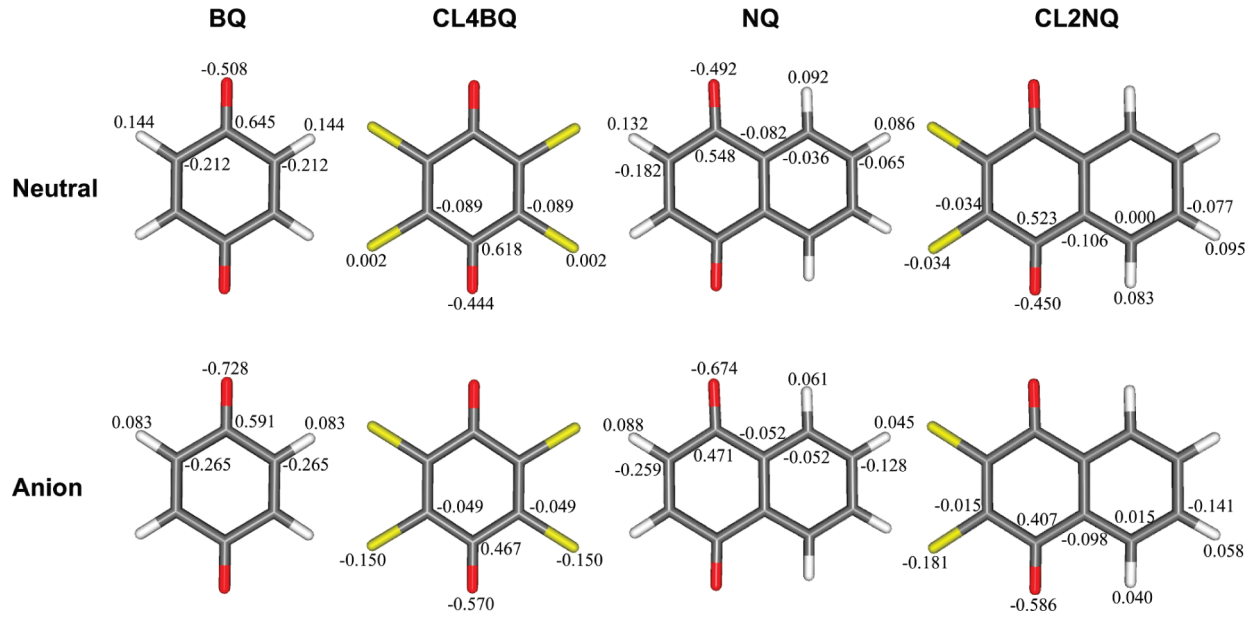

Figure 4. CHELPG atomic charges (in atomic units) for each species computed at the B3LYP/aug-cc-pVTZ level. Each molecule exhibits a horizontal mirror plane, and the unlabeled charges are determined by symmetry. Gray atoms correspond to carbon, white to hydrogen, red to oxygen, and yellow to chlorine.

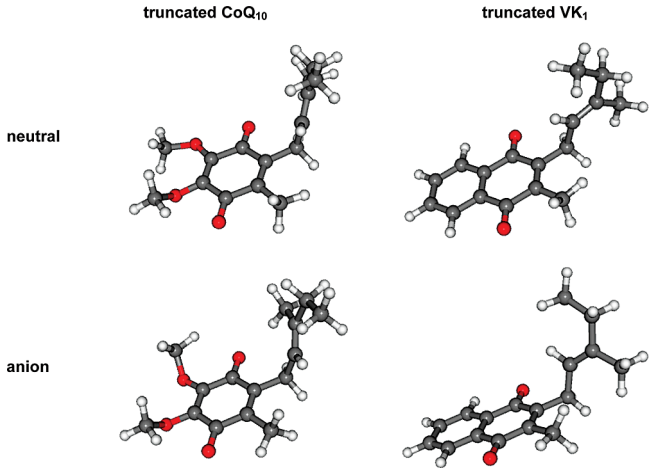

Figure 5. Optimized structures of CoQ_{10} and VK_1 (neutral and singly reduced) with truncated aliphatic chains. For all structures, the geometry optimization produced conformers with aliphatic and methoxy chains folded orthogonally to the ring planes. For the truncated CoQ_{10}, all three flexible chains (the aliphatic and the two methoxy substituents) were folded toward the same side of the ring plane.

double layer as a capacitor with a shunt resistor, R_{Sh}, and a series resistor, R_{Ser} (Figure 6a).[171] For the range of electrolyte concentrations that we used for the cyclic voltammetry measurements, that is, for $C_{Bu_4NPF_6}$between 100 and 300 mM, the IS data revealed a negligible correlation between the double-layer capacitance, C_{DL}, and $C_{Bu_4NPF_6}$ (Figure 6c). The values of C_{DL}, however, did manifest dependence on the potential of the working electrode (Figure 6c).

The observed lack of concentration dependence of the double-layer capacitance is consistent with the Gouy−Chapman−Stern model for surfaces submersed in concentrated electrolyte solutions.[171−173] At such high $C_{Bu_4NPF_6}$, the capacitance of the compact Stern layer has the predominant contribution to the reactance component of the measured impedance. The gradual potential-induced changes of C_{DL}, although not depicted by the Helmholtz approximation for the Stern layer capacitance, are consistent with alterations in the composition of the compact layer induced by charging and discharging of the working electrode.[174]

While the thickness and the composition of the diffuse layer depend strongly on the ionic charge and concentration, the compact layer is concentration-independent.[171] Furthermore, the Debye length, characteristic of the thickness of the diffuse layer, ranges between about 0.2 and 0.7 nm for the electrolyte concentrations that we used. Such short Debye lengths are smaller than the size of the electrolyte ions, making it meaningless to define a true diffuse layer. Therefore, beyond the compact layer, the quinone species at the electrode interface experience an environment comparable to that of the bulk electrolyte solutions. As a result, $E_{1}^{(1/2)}$ exhibited a pronounced dependence on $C_{Bu_4NPF_6}$, while C_{DL} was concentration-independent.

We have previously demonstrated the dependence of the redox potentials of other species on the dielectric properties of the electrolyte solutions.[42] Using similar analysis, we have estimated the effective radius of ferrocenium to be about 2.6 Å,[42] which was in agreement with the crystallographic radius, 2.7 Å, and the hydrodynamic radius, 3.2 Å, of ferrocene.[175−177] Apparently, such electrochemical analysis manifested the potential for yielding plausible results for the effective dimensions of redox species. Therefore, the principal reasons for the discrepancies observed for the investigated quinones should be sought in their structural features. Two important structural differences, however, set apart the quinones from ferrocene; (1) quinone molecules are planar, while the ferrocene chelate has a shape that can be approximated to a cylinder or a sphere, and (2) the charges of the quinone anions are localized predominantly on the peripheral oxygens (Figure 4), while the charge of the ferrocenium cation resides on the relatively large orbitals of the ferric ion, distributed around the center of the chelate.

Generalized Born Approach. To address the discrepancies between the measured and calculated quinone radii, we explored the generalized Born (GB) approach. The GB approach, rather than attempting to fit a molecule and its ions into a single sphere, treats the molecular species as a collection of spheres.[1,2,90−95]

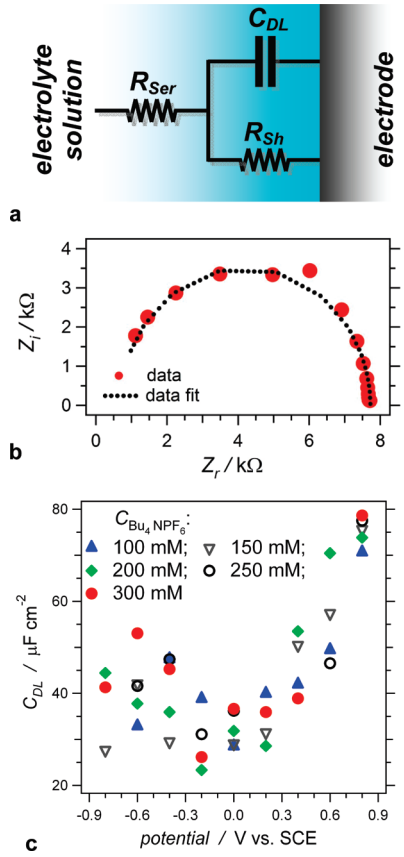

Figure 6. Impedance spectroscopy chloroform solutions of Bu_4NPF_6 with different concentrations. (a) Circuit representation of the electrical properties of the double layer on the working electrode in the absence of Faradaically active species; C_{DL} = double-layer capacitance, R_{Sh} = shunt resistance, and R_{Ser} = series resistance. (b) Nyquist plot of 150 mM Bu_4PF_6 at 0.6 V versus SCE. Z_r and Z_i are the real and imaginary components, respectively, of the impedance. The dotted line represents the Randles Model fit, that is, using the circuit model shown in (a). (c) Dependence of the double-layer capacitance on the applied potential for different electrolyte concentrations.

Representing each of the reduced and oxidized molecules as a collection of N atoms with atomic radii r_i and atomic charges z_i transforms their charge-to-size ratios, Ξ (eq 2a), into the corresponding GB forms[1,2]

$$\Xi^{(GB)} = e^2 \sum_{i=1}^{N} \sum_{j=1}^{N} \frac{z_i z_j}{f_{ij}} \tag{5a}$$

where $\sum_{i=1}^{N} z_i = Z - n$ and $\sum_{i=1}^{N} z_i = Z$ represent the total charge of the reduced and the oxidized species, respectively, and the GB parameter, f_{ij}, represents the corrected interatomic distance[1]

$$f_{ij} = \sqrt{d_{ij}^2 + \alpha_i \alpha_j \exp\left(-\frac{d_{ij}^2}{4\alpha_i \alpha_j}\right)} \tag{5b}$$

where d_{ij} is the center-to-center distance between atoms i and j, and α_i is the Born radius of atom i. For cases of nonoverlapping spheres, α_i can be expressed analytically[1]

$$\alpha_i^{-1} = r_i^{-1} - \sum_{\substack{j=1 \\ j \neq i}}^{N} \frac{r_j}{2(d_{ij}^2 - r_j^2)} - \sum_{\substack{j=1 \\ j \neq i}}^{N} \frac{1}{4d_{ij}} \log \frac{d_{ij} - r_j}{d_{ij} + r_j} \tag{5c}$$

where for r_i, we assumed the covalent radii, which we extracted from the atomic coordinates for the minimized structures of the quinones (Figure 4).[178] It should be noted that, although the oxidized form of the quinones is not charged, that is, $Z = 0$, the partial charges on the different atoms in the electroneutral molecules, that is, $z_i \neq 0$ (Figure 4, top row), result in nonzero values for their GB charge-to-size ratio, $\Xi_{Ox}^{(GB)}$ (eq 5a).

Apparently, the Born atomic radii, α_i, are larger than the corresponding covalent or van der Waals radii, r_i. As revealed by eq 5c, this difference between α_i and r_i is less pronounced for atoms located at the periphery of the molecule.

The classical Born expressions revealed that the slopes of the linear correlations between the measured reduction potentials, $E_1^{(1/2)}$, and the inverted dielectric constants of the media, $1 - \varepsilon^{-1}$ (Figure 3), should yield the difference between the charge-to-size ratios, $\Xi_{Red} - \Xi_{Ox}$ (eq 2a). This difference, $\Xi_{Red} - \Xi_{Ox}$, encompasses information about the measured effective radii, R_{eff}, of the electrochemically analyzed species (eqs 2b and 4). As we demonstrated, the thus-obtained values of R_{eff} from the experimental data, however, proved physically unfeasible to accommodate the spherical approximation adopted by the classical Born approach (Table 2).

Adopting physically feasible molecular geometries and charge distributions, the generalized Born approach allowed for estimation of the charge-to-size ratios, $\Xi_{Red}^{(GB)}$ and $\Xi_{Ox}^{(GB)}$, of the reduced and oxidized components of redox couples (eq 5). Concurrently, for the treatment of the experimental findings involving one-electron reduction, $n = 1$, of noncharged species, $Z = 0$, we equated the difference between the charge-to-size ratios with e^2/R_{eff} (eqs 2 and 4). As a corollary, it permitted extraction from the generalized Born approach values for the effective radii, $R_{eff}^{(GB)}$, expected to be observed for one-electron reduction of the investigated redox species

$$R_{eff}^{(GB)} = \frac{e^2}{\Xi_{Red}^{(GB)} - \Xi_{Ox}^{(GB)}} \tag{6}$$

A comparison between the experimental R_{eff} (eq 4) and the predicted $R_{eff}^{(GB)}$ (eq 6) values allowed us to test if the GB approach adequately addresses the discrepancy issues with the single-sphere approximation of the quinone ions.

In order to employ this GB approach, using ab initio calculations, we estimated the atomic charges and coordinates for the relaxed structures of four of the quinones and their anions. Molecular structures for the neutral and anionic versions of the four benzo- and naphthaquinones were optimized using the B3LYP density functional and the aug-cc-pVTZ basis set. Atomic point charges were determined using the CHELPG method, which determines a set of atomic charges that reproduce the molecular electrostatic potential at a large number of grid points around the molecule. The negative charges of the quinone radical ions were localized around the periphery of the molecules, predominantly on the oxygen atoms (Figure 4).

The calculated $R_{eff}^{(GB)}$ (eqs 5 and 6) manifested a closer agreement with the effective radii, R_{eff}, obtained from the redox potential analysis than the effective radii of the solvation spheres, R_{sph}, with R_{eff} (Table 2). The relative discrepancies between $R_{eff}^{(GB)}$

SCHEME 3: Hypothetical Molecular Ion with D_4 Symmetry Composed of Five Spheres

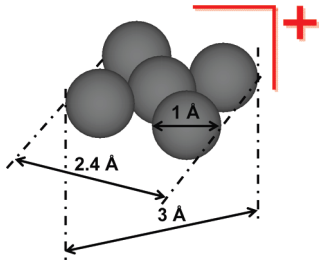

and R_{eff}, (i.e., $\Delta gb = |R_{eff} - R_{eff}^{(GB)}|R_{eff}^{-1}$) are 2−35-fold smaller than the relative discrepancies between $R_{sph}^{(Q^{\bullet-})}$ and R_{eff}, (i.e., $\Delta sph = |R_{eff} - R_{sph}^{(Q^{\bullet-})}|R_{eff}^{-1}$), as illustrated by the Δsph/Δgb ratios (Table 2). This finding suggested that it was most probably the spherical approximation of the molecular shapes that led to the observed discrepancy between the experimentally estimated effective radii and the feasible molecular dimensions.

The larger size of the CoQ10 and VK1 quinones makes B3LYP/aug-cc-pVTZ calculations too computationally expensive. Given the aforementioned ambiguity about the behavior of the long, flexible aliphatic chain in solution and the need to reduce the computational cost, we (1) truncated the chain to only six carbon atoms (Scheme 2) and (2) used the smaller 6-31+G(d) basis set to compute both the optimal geometry and CHELPG atomic charges. A series of control calculations determined that these two approximations have a relatively small impact on the predicted effective radii. First, using the 6-31+G(d) basis set for BQ and $BQ^{\bullet-}$, for example, yielded $R_{eff}^{(GB)}$ values that differed by less than 1% from the cc-pVTZ basis set calculations. Second, semiempirical AM1 geometry optimizations followed by B3LYP/aug-cc-pVDZ CHELPG atomic charge predictions on VK_1 with the truncated and complete aliphatic chains (Schemes 1 and 2) produced effective radii that differed by less than 10% from each other.

Compared to the other four quinones, CoQ_{10} and VK_1 manifested the much larger discrepancies between $R_{eff}^{(GB)}$ and R_{eff}, that is, the largest Δgb (Table 2). Our aforementioned control calculations suggest that these discrepancies are not due to the use of a smaller basis set or chain truncation in the calculations. Rather, we believe that they arise from the flexible nature of the aliphatic chains. The effective GB radii, $R_{eff}^{(GB)}$, strongly depend on the Born radii, α_i, of the comprising atomic spheres (eq 5c). A decrease in α_i of the atoms, on which the negative charges of the singly reduced quinones reside, results in a decrease in $R_{eff}^{(GB)}$. Gas-phase ab initio calculations yielded folded conformations of CoQ_{10} and VK_1 (Figure 5). Extended conformers (which are expected for solution media), however, provide an increase in the interatomic distances, d_{ij}, leading to a decrease in α_i (eq 5c) and, hence, a decrease in $R_{eff}^{(GB)}$. Therefore, the folded conformations underline a potential reason for the overestimated values of $R_{eff}^{(GB)}$ for CoQ_{10} and VK_1.

To further examine the role of the molecular shape and of the charge distribution on the effective radii of molecular ions, we employed the GB approach for a singly charged hypothetical molecule composed of five spheres arranged in a square, that is, D_4 symmetry (Scheme 3). Setting the diameter for each of the five spheres to 1 Å yielded the dimensions of the hypothetical molecule, that is, 2.4 × 2.4 × 1 Å (Scheme 3), which could fit into a spherical cavity with a radius of 1.5 Å. We applied the GB analysis to the hypothetical species in which the charge was localized on one of the five spheres or equally distributed between two, three, four, and five spheres with different configurations (Table 3).

The size of the hypothetical molecular ion was the same for all charge distributions, and hence, it should occupy the same solvent cavity. The GB effective radius, $R_{eff}^{(GB)}$, however, manifested a strong dependence on the patterns in which the charge was distributed among the five spheres (Table 3). For all cases, the values of the effective radii were 1.3- to 2.3-fold smaller than the 1.5 Å radius of the solvation spherical cavity that could accommodate the molecule (Table 3). For the cases of charge distribution over two of the five spheres, the effective radii of the hypothetical molecular anions were smaller when the two spheres carrying the charge were closer together. A similar trend was observed for the charge that was distributed over three and even over four spheres, that is, the values of $R_{eff}^{(GB)}$ were smaller when the charged spheres were next to one another (Table 3). These findings demonstrated that (1) nonspherical charged species have effective radii smaller that the radii of the spheres, in which they could fit, and (2) localization of the charges within the molecular entities leads to a decrease in the values of the effective radii of their ions.

The generalized Born approach is still an approximation. Defining atoms or functional groups as spheres, with homogeneous distribution of charge densities, presents a potentially crucial pitfall. For covalently bonded atoms, the charge density distribution does not necessarily have spherical symmetry. Furthermore, defining the boundaries of the electronic clouds that encompass the ionic charges (and hence, defining the effective ionic radii) is somewhat arbitrary. Nevertheless, the generalized Born approach presents a significant improvement over the single-sphere approximation. It has the potential ability to relate experimentally measurable quantities with physically feasible dimensions of charged molecular species.

Implications of Effective Radii for the Analysis of Charge-Transfer Systems. For semiclassical analyses of charge-transfer processes, information about the radii of the participating electron donors and acceptors is crucial. The effective radii are essential for estimating not only of the driving force of the process, via the Rehm−Weller equation,[40−42] but also of the outer-sphere reorganization energy.[179−181] Semiclassical dielectric continuum approaches, which were developed and confirmed for spherically symmetrical ions, have proven immensely indispensable for a wide range of charge-transfer studies and have demonstrated predictive capabilities.[3]

For organic moieties that are not spherically shaped, the estimation of the effective radii from experimental or from computational data is somewhat arbitrary. For example, for moieties that have elongated and/or flat shapes, such as quaterthiophenes and quinones, the effective diameters can be equated with the average of their length, width, and height in order to analyze charge-transfer kinetics.

As we demonstrated with the GB approach for the hypothetical ionic species (Scheme 3, Table 3), such effective radii, obtained from averaging of the three dimensions of the molecular ions, are plausible when the charges are evenly distributed over the whole molecular volume. Indeed, the average for 2.4 × 2.4 × 1 Å species is about 1.9 Å, the half of which agrees well with the 1 Å effective radii calculated for the cases of a charge distribution over four of five spheres (Table 3).

Charges localized within relatively small volumes at the periphery of the molecular ions, however, present potentials for significant discrepancies in the estimation of their effective radii directly from their molecular dimensions. Recently, we reported, for example, charge-transfer behavior of an acridinium−thiophene dyad, suggesting that the effective radius of the acridinium cation

TABLE 3: Generalized Born Effective Radius, $R_{eff}^{(GB)}$, of a Hypothetical Singly Charged Molecular Ion (Scheme 3) with Different Charge Distribution

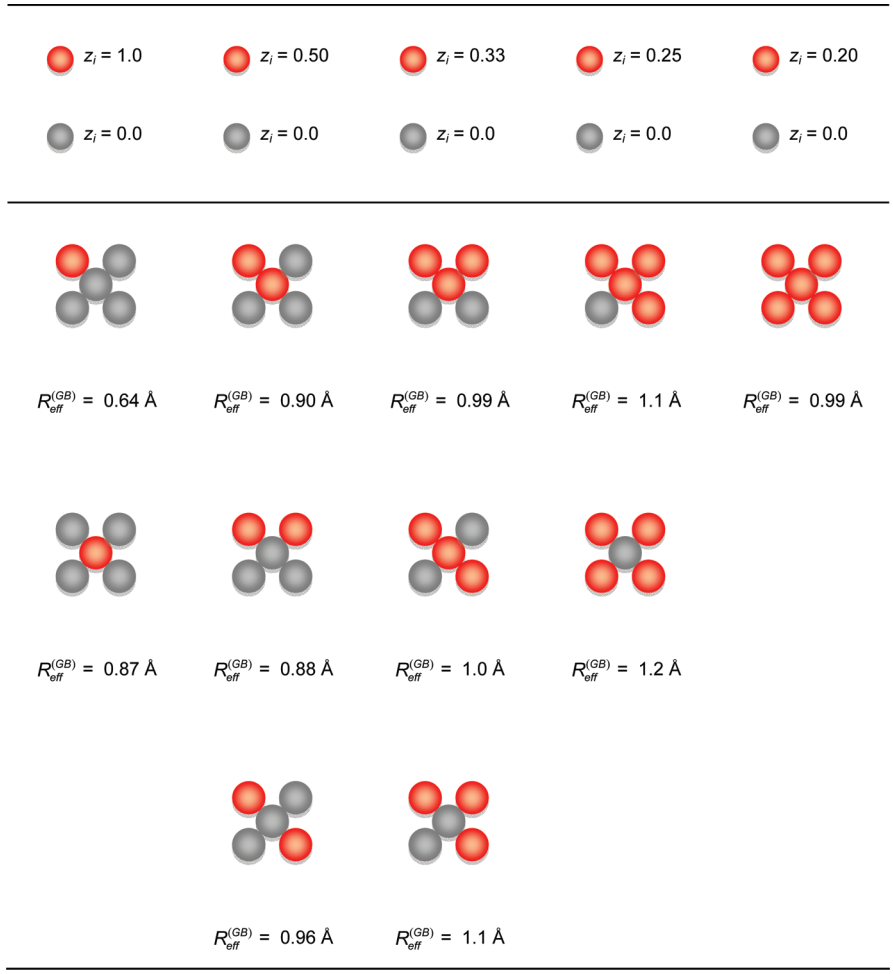

(comprising three condensed six-member rings) was smaller than that of the thiophene radical cation (comprising a single five-member ring).[80] The localization of the acridinium positive charge on its nitrogen heteroatom can provide an explanation for the observed trend.[82,83]

Quinones presented another example for effective radius discrepancies resultant from charge localization in nonspherically shaped species. The generalized Born approach, however, presented trends that tend to account for the charge localization in the estimation of the quinone effective radii (Table 2).

Conclusions

The values of the effective radii of charged organic moieties have a key importance for the estimation of the energetics of charge-transfer processes. The dielectric continuum treatment involving effective radii is important for estimation not only of the Born solvation term in the Rehm−Weller equation but also of the outer-sphere component of the reorganization energy. Therefore, the relation between the "true" molecular dimensions and the effective radii for the broadly used spherical approximation is crucial for semiclassical analysis of charge-transfer systems. The generalized Born approach allowed us to relate experimentally obtained effective radii of quinone derivatives with their structural and charge-distribution characteristics. We believe that such approaches, deviating from the single-sphere approximation, have the potential to provide means for analysis of redox processes involving moieties with irregular shapes and uneven charge density distributions.

Experimental Section

Materials. 1,4-Benzoquinone, 1,4-naphthoquinone, 2,3-dichloro-1,4-naphthoquinone, tetrachloro-1,4-benzoquinone, vitamin K_1, coenzyme Q_{10}, tetrabutylammonium hexafluorophosphate, 4-bromo-1,8-naphthalic anhydride, 3-dimethylaminopropanenitrile, 1,2-dimethoxyethane, acetic acid, and aniline were purchased from Sigma-Aldrich. Anhydrous solvents, chloroform, and acetonitrile, and spectroscopic-grade solvents, *n*-hexane, tetrachloromethane, chloroform, dichloromethane, benzonitrile, and dimethyl sulfoxide, were purchased from Fisher Scientific. *N*-phenyl-4-dimethylamino-1,8-naphthalimide (Ph-ANI) was prepared from 4-bromo-1,8-naphthalic anhydride, 3-dimethylaminopropanenitrile, and aniline via a two-step synthesis, as we have previously reported.[42]

Cyclic Voltammetry. The electrochemical measurements were conducted using Reference 600 Potentiostat/Galvanostat/ZRA (Gamry Instruments, PA, U.S.A.), equipped with a three-electrode cell. A glassy carbon electrode and platinum wire were used for the working and counterelectrodes, respectively. A saturated calomel electrode (Gamry Instruments) was used for a reference electrode. To prevent contamination, the reference electrode was brought into contact with the sample solutions via two salt bridges. To prevent drastic potential drops between the aqueous electrode media and the chloroform solutions, the solution between the two salt bridges was 100 mM tetrabutylammonium hexafluorophosphate in anhydrous acetonitrile. When not in use, the reference electrode was stored submersed in saturated potassium chloride solution. For all samples, the

quinone concentration was 2 mM. For each sample, the solution was purged with pure argon gas for 30 min, and at least five scans were recorded at a 50 mV/s scan rate.[18,42,182]

Impedance Spectroscopy. Impedance measurements were conducted using a Reference 600 Potentiostat/Galvanostat/ZRA (Gamry Instruments, PA, U.S.A.). The measurements were carried out by setting the AC voltage amplitude to 0.1 V while the applied DC potential ranged from −0.8 to 0.8 V versus SCE. Prior to the conductivity measurements, the working electrode surface was polished with alumina (0.05 μm grade, Buehler Ltd., U.S.A.) and thereafter cleaned in ethanol (200 proof, Fisher Scientific, U.S.A.) in an ultrasonic bath and dried by air. The impedance spectra of the double layer on the working electrode for different electrolyte concentrations were recorded at a frequency from 1 kHz to 1 MHz and fitted by the Randles Model.

Fluorescence Spectroscopy. Steady-state emission measurements were conducted using a FluoroLog-3 spectrofluorometer (Horiba−Jobin−Yvon) equipped with double-grating monochromators and a TBX single-photon-counting detector.[42,101,183−185] By adjusting the slit widths, the signal at all wavelengths was kept under 10^6 CPS to ensure that it was within the linear range of the detector. For all samples, the concentration of Ph-ANI was 10 μM.

Refractive Index Measurements. The refractive indices for the varying electrolyte concentrations were measured at 21 °C using Spectronic Instruments Refractometer model 334610. The reported values are averages of four individual readings. Different concentrations of electrolytes were prepared by mixing anhydrous chloroform with tetrabutylammonium hexafluorophosphate and sealed in dry sample vials until use.

Data Analysis. The values for the peak maxima (and minima) from the cyclic voltammograms and from the fluorescence spectra were obtained by fitting the region around the maxima (or the minima) to a Gaussian function. The fluorescence spectra of Ph-ANI were deconvoluted by fitting them to sums of Gaussian functions.[186,187] The quality of the fits was monitored by examination of the residuals. All least-squares data fits and the deconvolutions of fluorescence spectra were conducted using Igor Pro, version 6 (Wavematrics, Inc.), on MacOS and Windows XP workstations.[188−191]

Ab Initio Calculations. Density functional theory (DFT) calculations were performed using the B3LYP density functional.[192,193] For the anions, spin-unrestricted DFT was used. Initial results were obtained in the aug-cc-pVDZ basis.[194] For the generalized Born geometries and point charges, these were refined with the larger aug-cc-pVTZ basis set. For the truncated CoQ_{10} and VK_1 (Scheme 2), a reduced basis set, 6-31+G(d), was used. All calculations were performed using GAUSSIAN 03.[195]

Spherical radii for the molecules were computed in a two-step procedure. First, the molecular volume inside of a 0.001 electrons/Bohr^3 density contour was estimated using Monte Carlo integration, using 10 000 integration points. Each integration was repeated 100 times, and the resulting standard deviation for the calculated volumes was approximately 0.5%. Second, the spherical radius was estimated from the mean volume according to the scheme of Wong and co-workers.[170] In this scheme, the volume is scaled by a factor of 4/3. Then, the corresponding spherical radius is computed and increased by 0.5 Å. This empirical adjustment typically provides improved cavity sizes for implicit solvent models.[170] The standard deviation in the predicted spherical radii over the 100 runs per molecule is less than 0.01 Å.

For the generalized Born model, the neutral and anionic species for each of the four molecules were optimized separately. For each optimized structure, atomic charges were computed using the CHELPG scheme,[196] which fits charges to reproduce the molecular electrostatic potential at a series of grid points surrounding the molecule.

GB Calculations. The GB calculations (eqs 5 and 6) were conducted using macros written for Igor Pro, version 6 (Wavematrics, Inc.), run on MacOS. The atomic charges were obtained from the ab initio calculations (Figure 4) or estimated for equal distribution over the charged spheres of the hypothetical species (Table 3). The atomic radii, r_i, were estimated from the atomic coordinates of the minimized structures (Figure 4). In order to employ eq 5c, the radius of each atom, r_i, represents the maximum radius of a sphere (centered at the coordinates of the corresponding atom) that can fit within the molecular structure without overlapping with the spheres representing the neighboring atoms.

Acknowledgment. This research was supported by the National Science Foundation (CBET 0935995 and DBI 0731660) and by the U.C. Regents Faculty Development Award (V.V.). We also extend our gratitude to Dr. Rodney Jenks for his assistance with the refractive index measurements.

References and Notes

(1) Bashford, D.; Case, D. A. *Annu. Rev. Phys. Chem.* **2000**, *51*, 129–152.
(2) Still, W. C.; Tempczyk, A.; Hawley, R. C.; Hendrickson, T. *J. Am. Chem. Soc.* **1990**, *112*, 6127–6129.
(3) Marcus, R. A.; Sutin, N. *Biochim. Biophys. Acta* **1985**, *811*, 265–322.
(4) Gust, D.; Moore, T. A.; Moore, A. L. *Acc. Chem. Res.* **2009**, *42*, 1890–1898.
(5) Wasielewski, M. R. *Acc. Chem. Res.* **2009**, *42*, 1910–1921.
(6) Schuster, D. I.; Megiatto, J. D., Jr. *Nat. Chem.* **2009**, *1*, 182–183.
(7) Hambourger, M.; Moore, G. F.; Kramer, D. M.; Gust, D.; Moore, A. L.; Moore, T. A. *Chem. Soc. Rev.* **2009**, *38*, 25–35.
(8) van der Est, A. *Wiley Encycl. Chem. Biol.* **2009**, *3*, 676–682.
(9) Chen, F.; Tao, N. J. *Acc. Chem. Res.* **2009**, *42*, 429–438.
(10) Rosokha, S. V.; Kochi, J. K. *Acc. Chem. Res.* **2008**, *41*, 641–653.
(11) Piera, J.; Backvall, J. E. *Angew. Chem., Int. Ed.* **2008**, *47*, 3506–3523.
(12) Wasielewski, M. R. *J. Org. Chem.* **2006**, *71*, 5051–5066.
(13) Schuster, D. I.; Li, K.; Guldi, D. M. *C. R. Chim.* **2006**, *9*, 892–908.
(14) Seibert, M.; Wasielewski, M. R. *Ad. Photosynth. Respir.* **2005**, *20*, 269–274.
(15) Jones, G. L., II; Zhou, X.; Vullev, V. I. *Photochem. Photobiol. Sci.* **2003**, *2*, 1080–1087.
(16) Vullev, V. I.; Jones, G., II. *Res. Chem. Intermed.* **2002**, *28*, 795–815.
(17) Bracher, P. J.; Schuster, D. I. *Dev. Fullerene Sci.* **2002**, *4*, 163–212.
(18) Jones, G., II; Vullev, V. I. *Org. Lett.* **2002**, *4*, 4001–4004.
(19) Lukas, A. S.; Wasielewski, M. R. *Electron Transfer Chem.* **2001**, *5*, 48–96.
(20) Jones, G., II; Vullev, V.; Braswell, E. H.; Zhu, D. *J. Am. Chem. Soc.* **2000**, *122*, 388–389.
(21) Jones, G., II; Lu, L. N.; Vullev, V.; Gosztola, D.; Greenfield, S.; Wasielewski, M. *Bioorg. Med. Chem. Lett.* **1995**, *5*, 2385–2390.
(22) Newton, M. D. *Chem. Rev.* **1991**, *91*, 767–792.
(23) Wasielewski, M. R.; Niemczyk, M. P.; Svec, W. A.; Pewitt, E. B. *Springer Ser. Chem. Phys.* **1985**, *42*, 242–249.
(24) Siegbahn, P. E. M. *Acc. Chem. Res.* **2009**, *42*, 1871–1880.
(25) Davidson, V. L. *Acc. Chem. Res.* **2008**, *41*, 730–738.
(26) Rosenberg, E.; Koren, O.; Reshef, L.; Efrony, R.; Zilber-Rosenberg, I. *Nat. Rev. Microbiol.* **2007**, *5*, 355–362.
(27) Rascher, U.; Nedbal, L. *Curr. Opin. Plant Biol.* **2006**, *9*, 671–678.
(28) Iverson, T. M. *Curr. Opin. Chem. Biol.* **2006**, *10*, 91–100.
(29) Chergui, M. *Science* **2006**, *313*, 1246–1247.
(30) Szacilowski, K.; Macyk, W.; Drzewiecka-Matuszek, A.; Brindell, M.; Stochel, G. *Chem. Rev.* **2005**, *105*, 2647–2694.
(31) Fagnoni, M.; Albini, A. *Acc. Chem. Res.* **2005**, *38*, 713–721.

(32) Gratzel, M. *Acc. Chem. Res.* **2009**, *42*, 1788–1798.
(33) Kaneko, M. *Springer Ser. Mater. Sci.* **2009**, *111*, 199–215.
(34) Heremans, P.; Cheyns, D.; Rand, B. P. *Acc. Chem. Res.* **2009**, *42*, 1740–1747.
(35) Sirimanne, P. M.; Perera, V. P. S. *Phys. Status Solidi B.* **2008**, *245*, 1828–1833.
(36) Andrews, D. L. *Journal of Nanophotonics* **2008**, *2*, 022502.
(37) Gratzel, M. *Philos. Trans. R. Soc. London, Ser. A* **2007**, *365*, 993–1005.
(38) Blom, P. W. M.; Mihailetchi, V. D.; Koster, L. J. A.; Markov, D. E. *Adv. Mater.* **2007**, *19*, 1551–1566.
(39) Graetzel, M. *C. R. Chim.* **2006**, *9*, 578–583.
(40) Rehm, D.; Weller, A. *Isr. J. Chem.* **1970**, *8*, 259–271.
(41) Braslavsky, S. E.; Acuna, A. U.; Adam, W.; Amat, F.; Armesto, D.; Atvars, T. D. Z.; Bard, A.; Bill, E.; Bjoern, L. O.; Bohne, C.; Bolton, J.; Bonneau, R.; Bouas-Laurent, H.; Braun, A. M.; Dale, R.; Dill, K.; Doepp, D.; Duerr, H.; Fox, M. A.; Gandolfi, T.; Grabowski, Z. R.; Griesbeck, A.; Kutateladze, A.; Litter, M.; Lorimer, J.; Mattay, J.; Michl, J.; Miller, R. J. D.; Moggi, L.; Monti, S.; Nonell, S.; Ogilby, P.; Olbrich, G.; Oliveros, E.; Olivucci, M.; Orellana, G.; Prokorenko, V.; Naqvi, K. R.; Rettig, W.; Rizzi, A.; Rossi, R. A.; San Roman, E.; Scandola, F.; Schneider, S.; Thulstrup, E. W.; Valeur, B.; Verhoeven, J.; Warman, J.; Weiss, R.; Wirz, J.; Zachariasse, K. *Pure Appl. Chem.* **2007**, *79*, 293–465.
(42) Bao, D.; Millare, B.; Xia, W.; Steyer, B. G.; Gerasimenko, A. A.; Ferreira, A.; Contreras, A.; Vullev, V. I. *J. Phys. Chem. A* **2009**, *113*, 1259–1267.
(43) Born, M. *Z. Phys.* **1920**, *1*, 45–48.
(44) Rashin, A. A.; Honig, B. *Ann. N.Y. Acad. Sci.* **1986**, *482*, 143–144.
(45) Sinha, B.; Roy, P. K.; Sarkar, B. K.; Brahman, D.; Roy, M. N. *J. Chem. Thermodyn.* **2010**, *42*, 380–386.
(46) Yadava, S. S.; Yadav, A.; Kushwaha, N.; Yadav, N. *Indian J. Chem., Sect. A: Inorg., Bio-inorg., Phys., Theor. Anal. Chem.* **2009**, *48A*, 650–657.
(47) Jakli, G. *J. Chem. Eng. Data* **2009**, *54*, 2656–2665.
(48) Cibulka, I.; Hnedkovsky, L.; Sedlbauer, J. *J. Chem. Thermodyn.* **2009**, *42*, 198–207.
(49) Tjahjono, M.; Garland, M. *J. Solution Chem.* **2007**, *36*, 221–236.
(50) Mallick, B. C.; Kishore, N. *J. Solution Chem.* **2006**, *35*, 1441–1451.
(51) Pandey, J. D.; Dey, R.; Datt Bhatt, B. *J. Mol. Liq.* **2004**, *111*, 67–71.
(52) Raos, N. *Croat. Chem. Acta* **2003**, *76*, 81–85.
(53) Elkashef, H. *Opt. Mater.* **1997**, *8*, 175–183.
(54) Aminabhavi, T. M.; Aralaguppi, M. I.; Harogoppad, S. B.; Balundgi, R. H. *Indian J. Technol.* **1993**, *31*, 27–31.
(55) Aminabhavi, T. M.; Aralaguppi, M. I.; Harogoppad, S. B.; Balundgi, R. H. *Indian J. Technol.* **1993**, *31*, 32–36.
(56) Aminabhavi, T. M.; Aralaguppi, M. I. *Indian J. Technol.* **1993**, *31*, 801–807.
(57) Swaddle, T. W.; Mak, M. K. S. *Can. J. Chem.* **1983**, *61*, 473–480.
(58) Tsierkezos, N. G.; Philippopoulos, A. I. *Fluid Phase Equilib.* **2009**, *277*, 20–28.
(59) Kuznetsova, E. M. *Russ. J. Phys. Chem.* **2005**, *79*, 1165–1168.
(60) Ue, M. *J. Electrochem. Soc.* **1996**, *143*, L270–L272.
(61) Crouch, E.; Persson, A.; Chang, D.; Heuser, J. *J. Biol. Chem.* **1994**, *269*, 17311–17319.
(62) Lim, S. K.; Burba, M. E.; Albrecht, A. C. *Chem. Phys. Lett.* **1993**, *216*, 405–408.
(63) Shimada, E.; Matsumura, G. *J. Chromatogr.* **1992**, *627*, 43–50.
(64) Schiller, R. *Radiat. Phys. Chem.* **1991**, *37*, 549–550.
(65) Kapinus, E. I.; Dilung, I. I. *Chem. Phys. Lett.* **1990**, *174*, 75–79.
(66) Pau, P. C. F.; Berg, J. O.; McMillan, W. G. *J. Phys. Chem.* **1990**, *94*, 2671–2679.
(67) Heyrovska, R. *Chem. Phys. Lett.* **1989**, *163*, 207–211.
(68) Ribela, M. T.; Bartolini, P. *Anal. Biochem.* **1988**, *174*, 693–697.
(69) Ibuki, K.; Nakahara, M. *J. Phys. Chem.* **1986**, *90*, 6362–6365.
(70) Fawcett, W. R.; Jaworski, J. S. *J. Phys. Chem.* **1983**, *87*, 2972–2976.
(71) Gill, D. S. *Electrochim. Acta* **1977**, *22*, 491–492.
(72) Nakagawa, S.; Takehara, Z.; Yoshizawa, S. *Electrochim. Acta* **1973**, *18*, 1043–1044.
(73) Waldmann-Meyer, H. *Biochim. Biophys. Acta* **1972**, *261*, 148–160.
(74) Rodbard, D.; Chrambach, A. *Anal. Biochem.* **1971**, *40*, 95–134.
(75) Bousfield, W. R. *Philos. Trans. R. Soc. London* **1906**, *206*, 101–159.
(76) Zhan, C.-G.; Chipman, D. M. *J. Chem. Phys.* **1998**, *109*, 10543–10558.
(77) Medina-Llanos, C.; Ågren, H.; Mikkelsen, K. V.; Jensen, H. J. A. *J. Chem. Phys.* **1989**, *90*, 6422–6435.
(78) McCreery, J. H.; Christoffersen, R. E.; Hall, G. G. *J. Am. Chem. Soc.* **1976**, *98*, 7191–7197.
(79) Rüssel, C.; Jaenicke, W. *J. Electroanal. Chem. Interfacial Electrochem.* **1984**, *180*, 205–217.
(80) Hu, J.; Xia, B.; Bao, D.; Ferreira, A.; Wan, J.; Jones, G.; Vullev, V. I. *J. Phys. Chem. A* **2009**, *113*, 3096–3107.
(81) Jones, G., II; Yan, D.; Hu, J.; Wan, J.; Xia, B.; Vullev, V. I. *J. Phys. Chem. B* **2007**, *111*, 6921–6929.
(82) Seiffert, W.; Limbach, H. H.; Zanker, V.; Mantsch, H. *Tetrahedron* **1970**, *26*, 2663–2675.
(83) Nishimoto, K.; Nakatsukasa, K.; Fujishiro, R.; Kato, S. *Theor. Chim. Acta* **1969**, *14*, 80–90.
(84) Karelson, M. M.; Zerner, M. C. *J. Phys. Chem.* **1992**, *96*, 6949–6957.
(85) Rinaldi, D.; Rivail, J. L.; Rguini, N. *J. Comput. Chem.* **1992**, *13*, 675–680.
(86) Harrison, S. W.; Nolte, H. J.; Beveridge, D. L. *J. Phys. Chem.* **1976**, *80*, 2580–2585.
(87) Huron, M. J.; Claverie, P. *J. Phys. Chem.* **1972**, *76*, 2123–2133.
(88) Lee, B.; Richards, F. M. *J. Mol. Biol.* **1971**, *55*, 379–400.
(89) Kirkwood, J. G.; Westheimer, F. H. *J. Chem. Phys.* **1938**, *6*, 506–512.
(90) Banks, J. L.; Beard, H. S.; Cao, Y.; Cho, A. E.; Damm, W.; Farid, R.; Felts, A. K.; Halgren, T. A.; Mainz, D. T.; Maple, J. R.; Murphy, R.; Philipp, D. M.; Repasky, M. P.; Zhang, L. Y.; Berne, B. J.; Friesner, R. A.; Gallicchio, E.; Levy, R. M. *J. Comput. Chem.* **2005**, *26*, 1752–1780.
(91) Chen, J.; Brooks, C. L., III; Khandogin, J. *Curr. Opin. Struct. Biol.* **2008**, *18*, 140–148.
(92) Constanciel, R.; Contreras, R. *Theor. Chim. Acta* **1984**, *65*, 1–11.
(93) Feig, M.; Brooks, C. L. *Curr. Opin. Struct. Biol.* **2004**, *14*, 217–224.
(94) Felts, A. K.; Gallicchio, E.; Wallqvist, A.; Levy, R. M. *Proteins: Struct., Funct., Genet.* **2002**, *48*, 404–422.
(95) Hawkins, G. D.; Cramer, C. J.; Truhlar, D. G. *J. Phys. Chem.* **1996**, *100*, 19824–19839.
(96) Heinis, T.; Chowdhury, S.; Scott, S. L.; Kebarle, P. *J. Am. Chem. Soc.* **1988**, *110*, 400–407.
(97) Kebarle, P.; Chowdhury, S. *Chem. Rev.* **1987**, *87*, 513–534.
(98) Jaworski, J. S. *Chem. Phys. Lett.* **1986**, *127*, 133–135.
(99) Peover, M. E. *Nature* **1962**, *193*, 475–476.
(100) Freguia, S.; Tsujimura, S.; Kano, K. *Electrochim. Acta* **2009**, *55*, 813–818.
(101) Wan, J.; Ferreira, A.; Xia, W.; Chow, C. H.; Takechi, K.; Kamat, P. V.; Jones, G.; Vullev, V. I. *J. Photochem. Photobiol., A* **2008**, *197*, 364–374.
(102) Sumida, J. P.; Liddell, P. A.; Lin, S.; Macpherson, A. N.; Seely, G. R.; Moore, A. L.; Moore, T. A.; Gust, D. *J. Phys. Chem. A* **1998**, *102*, 5512–5519.
(103) Kuciauskas, D.; Liddell, P. A.; Hung, S.-C.; Lin, S.; Stone, S.; Seely, G. R.; Moore, A. L.; Moore, T. A.; Gust, D. *J. Phys. Chem. B* **1997**, *101*, 429–440.
(104) Macpherson, A. N.; Liddell, P. A.; Lin, S.; Noss, L.; Seely, G. R.; DeGraziano, J. M.; Moore, A. L.; Moore, T. A.; Gust, D. *J. Am. Chem. Soc.* **1995**, *117*, 7202–7212.
(105) Sakata, Y.; Tsue, H.; O'Neil, M. P.; Wiederrecht, G. P.; Wasielewski, M. R. *J. Am. Chem. Soc.* **1994**, *116*, 6904–6909.
(106) Wasielewski, M. R.; Gaines, G. L., III; Wiederrecht, G. P.; Svec, W. A.; Niemczyk, M. P. *J. Am. Chem. Soc.* **1993**, *115*, 10442–10443.
(107) Johnson, D. G.; Niemczyk, M. P.; Minsek, D. W.; Wiederrecht, G. P.; Svec, W. A.; Gaines, G. L., III; Wasielewski, M. R. *J. Am. Chem. Soc.* **1993**, *115*, 5692–5701.
(108) Wasielewski, M. R.; O'Neil, M. P.; Gosztola, D.; Niemczyk, M. P.; Svec, W. A. *Pure Appl. Chem.* **1992**, *64*, 1319–1325.
(109) Seta, P.; Bienvenue, E.; Moore, A. L.; Mathis, P.; Bensasson, R. V.; Liddell, P.; Pessiki, P. J.; Joy, A.; Moore, T. A.; Gust, D. *Nature* **1985**, *316*, 653–655.
(110) Roessler, M. M.; King, M. S.; Robinson, A. J.; Armstrong, F. A. *Proc. Natl. Acad. Sci. U.S.A.* **2010**, *1*−*6*, 6.
(111) Hirst, J. *Biochem. J.* **2010**, *425*, 327–339.
(112) Uchimiya, M.; Stone, A. T. *Chemosphere* **2009**, *77*, 451–458.
(113) Nabedryk, E.; Breton, J. *Biochim. Biophys. Acta* **2008**, *1777*, 1229–1248.
(114) Savitsky, A.; Moebius, K. *Helv. Chim. Acta* **2006**, *89*, 2544–2589.
(115) Wraight, C. A. *Biophys. Struct. Aspects Bioenerg.* **2005**, 273–313.
(116) Semenov, A.; Cherepanov, D.; Mamedov, M. *Photosynth. Res.* **2008**, *98*, 121–130.
(117) Renger, G.; Renger, T. *Photosynth. Res.* **2008**, *98*, 53–80.
(118) Kirchhoff, H. *Biochem. Soc. Trans.* **2008**, *36*, 967–970.
(119) DeRuyter, Y. S.; Fromme, P. *Cyanobacteria* **2008**, 217–269.
(120) Lichtenthaler, H. K. *Photosynth. Res.* **2007**, *92*, 163–179.

(121) Xiong, L.; Seibert, M.; Gusev, A. V.; Wasielewski, M. R.; Hemann, C.; Hille, C. R.; Sayre, R. T. *J. Phys. Chem. B* **2004**, *108*, 16904–16911.
(122) Gunner, M. R.; Madeo, J.; Zhu, Z. *J. Bioenerg. Biomembr.* **2008**, *40*, 509–519.
(123) Wraight, C. A., *Photosynthesis: Mechanisms and Effects*, Proceedings of the International Congress on Photosynthesis, 11th, Budapest, Aug. 17−22, 1998; Kluwer Academic Publishers: Dordrecht, The Netherlands; Vol. 2, pp 693−698.
(124) Laible, P. D.; Zhang, Y.; Morris, A. L.; Snyder, S. W.; Ainsworth, C.; Greenfield, S. R.; Wasielewski, M. R.; Parot, P.; Schoepp, B.; Schiffer, M.; Hanson, D. K.; Thurnauer, M. C. *Photosynth. Res.* **1997**, *52*, 93–103.
(125) Breton, J.; Nabedryk, E. *Biochim. Biophys. Acta* **1996**, *1275*, 84–90.
(126) Shinkarev, V. P.; Wraight, C. A. *Photosynth. React. Cent.* **1993**, *1*, 193–255.
(127) Lenaz, G.; Genova, M. L. *Int. J. Biochem. Cell Biol.* **2009**, *41*, 1750–1772.
(128) Lenaz, G.; Genova, M. L. *Biochim. Biophys. Acta* **2009**, *1787*, 563–573.
(129) Genova, M. L.; Baracca, A.; Biondi, A.; Casalena, G.; Faccioli, M.; Falasca, A. I.; Formiggini, G.; Sgarbi, G.; Solaini, G.; Lenaz, G. *Biochim. Biophys. Acta* **2008**, *1777*, 740–746.
(130) Lenaz, G.; Fato, R.; Formiggini, G.; Genova, M. L. *Mitochondrion* **2007**, *7*, S8–S33.
(131) Zhu, L.; Wang, B.; Tan, J.; Luo, M. *Int. J. Cancer Res.* **2006**, *2*, 290–298.
(132) Genova, M. L.; Bianchi, C.; Lenaz, G. *BioFactors* **2005**, *25*, 5–20.
(133) Quinzii, C. M.; Lpez, L. C.; Naini, A.; DiMauro, S.; Hirano, M. *BioFactors* **2008**, *32*, 113–118.
(134) Spindler, M.; Beal, M. F.; Henchcliffe, C. *Neuropsychiatr. Dis. Treat.* **2009**, *5*, 597–610.
(135) Kumar, A.; Kaur, H.; Devi, P.; Mohan, V. *Pharmacol. Ther.* **2009**, *124*, 259–268.
(136) DiMauro, S.; Rustin, P. *Biochim. Biophys. Acta* **2009**, *1792*, 1159–1167.
(137) Schneider, C. B.; Storch, A. *Agro Food Ind. Hi-Tech* **2008**, *19*, 11–13.
(138) Henchcliffe, C.; Beal, M. F. *Nat. Clin. Pract. Neurol.* **2008**, *4*, 600–609.
(139) Hargreaves, I. P.; Lane, A.; Sleiman, P. M. A. *Neurosci. Lett.* **2008**, *447*, 17–19.
(140) Chaturvedi, R. K.; Beal, M. F. *Ann. N.Y. Acad. Sci.* **2008**, *1147*, 395–412.
(141) Littarru, G. P.; Tiano, L. *Mol. Biotechnol.* **2007**, *37*, 31–37.
(142) Li, W.; Schulman, S.; Dutton, R. J.; Boyd, D.; Beckwith, J.; Rapoport, T. A. *Nature* **2010**, *463*, 507–512.
(143) Wallin, R.; Wajih, N.; Hutson, S. M. *Vitam. Horm.* **2008**, *78*, 227–246.
(144) Berkner, K. L. *Vitam. Horm.* **2008**, *78*, 131–156.
(145) Benzakour, O. *Thromb. Haemostasis* **2008**, *100*, 527–529.
(146) Booth, S. L. *Annu. Rev. Nutr.* **2009**, *29*, 89–110.
(147) Rubinacci, A. *Am. J. Physiol.* **2009**, *297*, C1336–C1338.
(148) Krueger, T.; Westenfeld, R.; Schurgers, L. J.; Brandenburg, V. M. *Int. J. Artif. Organs* **2009**, *32*, 67–74.
(149) Gorter de Vries, I.; Wisse, E.; Williamson, M. K.; Price, P. A. *Calcif. Tissue Int.* **1991**, *49*, 355–358.
(150) Price, P. A.; Fraser, J. D.; Metz-Virca, G. *Proc. Natl. Acad. Sci. U.S.A.* **1987**, *84*, 8335–8339.
(151) Hui, Y.; Chng, E. L. K.; Chng, C. Y. L.; Poh, H. L.; Webster, R. D. *J. Am. Chem. Soc.* **2009**, *131*, 1523–1534.
(152) Quan, M.; Sanchez, D.; Wasylkiw, M. F.; Smith, D. K. *J. Am. Chem. Soc.* **2007**, *129*, 12847–12856.
(153) Rüssel, C.; Jaenicke, W. *J. Electroanal. Chem. Interfacial Electrochem.* **1986**, *199*, 139–151.
(154) Gestblom, B.; Svorstøl, I.; Songstad, J. *J. Phys. Chem.* **1986**, *90*, 4684–4686.
(155) Plakidin, V. L.; Vostrova, V. N. *Zh. Org. Khim.* **1981**, *17*, 1118–1119.
(156) Plakidin, V. L.; Vostrova, V. N. *Zh. Org. Khim.* **1983**, *19*, 2591–2600.
(157) Grabowski, Z. R.; Rotkiewicz, K.; Rettig, W. *Chem. Rev.* **2003**, *103*, 3899–4031.
(158) Rettig, W. *Top. Curr. Chem.* **1994**, *169*, 253–299.
(159) Rettig, W. *Angew. Chem.* **1986**, *98*, 969–986.
(160) Grabowski, Z. R.; Dobkowski, J. *Pure Appl. Chem.* **1983**, *55*, 245–252.
(161) Knyazhanskii, M. I.; Metelitsa, A. V.; Alekseev, Y. E.; Pyshchev, A. I.; Kovaleva, T. V.; Sudareva, T. P.; Uzhinov, B. M. *Russ. J. Org. Chem. (Transl. of Zh. Org. Khim.)* **2000**, *36*, 1192–1197.
(162) Alekseev, Y. E.; Knyazhanskii, M. I.; Metelitsa, A. V.; Sudareva, T. P.; Zhdanov, Y. A. *Dokl. Akad. Nauk* **2000**, *370*, 190–192.
(163) Jaworski, J. S.; Lesniewska, E.; Kalinowski, M. K. *J. Electroanal. Chem. Interfacial Electrochem.* **1979**, *105*, 329–334.
(164) Gutmann, V. *Electrochim. Acta* **1976**, *21*, 661–670.
(165) Mayer, U.; Gutmann, V.; Gerger, W. *Monatsh. Chem.* **1975**, *106*, 1235–1257.
(166) Gutmann, V.; Wychera, E. *Inorg. Nucl. Chem. Lett.* **1966**, *2*, 257–260.
(167) Shraydeh, B. F.; Zatar, N. *Monatsh. Chem.* **1994**, *125*, 655–659.
(168) Toma, H. E.; Takasugi, M. S. *J. Solution Chem.* **1989**, *18*, 575–583.
(169) Erlich, R. H.; Popov, A. I. *J. Am. Chem. Soc.* **1971**, *93*, 5620–5623.
(170) Wong, M. W.; Wiberg, K. B.; Frisch, M. J. *J. Comput. Chem.* **1995**, *16*, 385–394.
(171) Bard, A. J.; Faulkner, L. R. *Electrochemical Methods: Fundamentals and Applications*; John Wiley & Sons, Inc., 2001.
(172) Henderson, D.; Boda, D. *Phys. Chem. Chem. Phys.* **2009**, *11*, 3822–3830.
(173) Chattoraj, D. K. *J. Indian Chem. Soc.* **2009**, *86*, 1009–1017.
(174) Hahn, M.; Baertschi, M.; Barbieri, O.; Sauter, J. C.; Kotz, R.; Gallay, R. *Electrochem. Solid-State Lett.* **2003**, *7*, A33–A36.
(175) Laoire, C. O.; Plichta, E.; Hendrickson, M.; Mukerjee, S.; Abraham, K. M. *Electrochim. Acta* **2009**, *54*, 6560–6564.
(176) Shotwell, J. B.; Flowers, R. A., III. *Electroanalysis* **2000**, *12*, 223–226.
(177) Armstrong, N. R.; Quinn, R. K.; Vanderborgh, N. E. *Anal. Chem.* **1974**, *46*, 1759–1764.
(178) Pyykkö, P.; Atsumi, M. *Chem.−Eur. J.* **2009**, *15*, 186–197.
(179) Ayala, R.; Sprik, M. *J. Phys. Chem. B* **2008**, *112*, 257–269.
(180) Liu, Y.-P.; Newton, M. D. *J. Phys. Chem.* **1994**, *98*, 7162–7169.
(181) Brunschwig, B. S.; Ehrenson, S.; Sutin, N. *J. Phys. Chem.* **1986**, *90*, 3657–3668.
(182) Vullev, V. I.; Jones, G. *Tetrahedron Lett.* **2002**, *43*, 8611–8615.
(183) Thomas, M.; Wan, J.; Vullev, V. I. *AIP Conf. Proc.* **2009**, *1140*, 120–126.
(184) Vasquez, J. M.; Vu, A.; Schultz, J. S.; Vullev, V. I. *Biotechnol. Prog.* **2009**, *25*, 906–914.
(185) Wan, J.; Thomas, M. S.; Guthrie, S.; Vullev, V. I. *Ann. Biomed. Eng.* **2009**, *37*, 1190–1205.
(186) Jones, G., II; Vullev, V. I. *Photochem. Photobiol. Sci.* **2002**, *1*, 925–933.
(187) Jones, G., II; Vullev, V. I. *J. Phys. Chem. A* **2002**, *106*, 8213–8222.
(188) Vullev, V. I.; Wan, J.; Heinrich, V.; Landsman, P.; Bower, P. E.; Xia, B.; Millare, B.; Jones, G., II *J. Am. Chem. Soc.* **2006**, *128*, 16062–16072.
(189) Hong, C.; Bao, D.; Thomas, M. S.; Clift, J. M.; Vullev, V. I. *Langmuir* **2008**, *24*, 8439–8442.
(190) Millare, B.; Thomas, M.; Ferreira, A.; Xu, H.; Holesinger, M.; Vullev, V. I. *Langmuir* **2008**, *24*, 13218–13224.
(191) Thomas, M. S.; Clift, J. M.; Millare, B.; Vullev, V. I. *Langmuir* **2010**, *26*, 2951–2957.
(192) Becke, A. D. *J. Chem. Phys.* **1993**, *98*, 5648–5652.
(193) Lee, C.; Yang, W.; Parr, R. G. *Phys. Rev. B* **1988**, *37*, 785–789.
(194) Dunning, T. H., Jr. *J. Chem. Phys.* **1989**, *90*, 1007–1023.
(195) Frisch, M. J.; Trucks, G. W.; Schlegel, H. B.; Scuseria, G. E.; Robb, M. A.; Cheeseman, J. R.; Montgomery, J. A., Jr.; Vreven, T.; Kudin, K. N.; Burant, J. C.; Millam, J. M.; Iyengar, S. S.; Tomasi, J.; Barone, V.; Mennucci, B.; Cossi, M.; Scalmani, G.; Rega, N.; Petersson, G. A.; Nakatsuji, H.; Hada, M.; Ehara, M.; Toyota, K.; Fukuda, R.; Hasegawa, J.; Ishida, M.; Nakajima, T.; Honda, Y.; Kitao, O.; Nakai, H.; Klene, M.; Li, X.; Knox, J. E.; Hratchian, H. P.; Cross, J. B.; Bakken, V.; Adamo, C.; Jaramillo, J.; Gomperts, R.; Stratmann, R. E.; Yazyev, O.; Austin, A. J.; Cammi, R.; Pomelli, C.; Ochterski, J. W.; Ayala, P. Y.; Morokuma, K.; Voth, G. A.; Salvador, P.; Dannenberg, J. J.; Zakrzewski, V. G.; Dapprich, S.; Daniels, A. D.; Strain, M. C.; Farkas, O.; Malick, D. K.; Rabuck, A. D.; Raghavachari, K.; Foresman, J. B.; Ortiz, J. V.; Cui, Q.; Baboul, A. G.; Clifford, S.; Cioslowski, J.; Stefanov, B. B.; Liu, G.; Liashenko, A.; Piskorz, P.; Komaromi, I.; Martin, R. L.; Fox, D. J.; Keith, T.; Al-Laham, M. A.; Peng, C. Y.; Nanayakkara, A.; Challacombe, M.; Gill, P. M. W.; Johnson, B.; Chen, W.; Wong, M. W.; Gonzalez, C.; Pople, J. A. *Gaussian 03*, revision E.01; Gaussian, Inc.: Wallingford, CT, 2004.
(196) Breneman, C. M.; Wiberg, K. B. *J. Comput. Chem.* **1990**, *11*, 361–373.

JP101730E